Soft Matter

PAPER

View Article Online
View Journal | View Issue

Cite this: *Soft Matter*, 2018, **14**, 7045

A supramolecular hydrogel prepared from a thymine-containing artificial nucleolipid: study of assembly and lyotropic mesophases†

Dawei Zhang,[ab] Qingkun Liu,[c] Rayshan Visvanathan,[bc] Michael R. Tuchband,[c] Ghadah H. Sheetah,[bc] Benjamin D. Fairbanks,[a] Noel A. Clark,[c] Ivan I. Smalyukh[bc] and Christopher N. Bowman*[ab]

Received 6th July 2018,
Accepted 2nd August 2018

DOI: 10.1039/c8sm01383g

rsc.li/soft-matter-journal

An artificial nucleolipid containing thymine, a triazole-ring, and phosphatidylcholine (TTPC) moieties was prepared by copper catalyzed azide alkyne cycloaddition (CuAAC) under aqueous conditions. The resulting TTPC molecules assembled *in situ* into a fibrous aggregation. The study of the TTPC fiber assembly using XRD and NMR spectroscopy revealed that the formation of fibers was driven by the unique combination of the lipid and nucleobase moieties in the structure of TTPC. At a critical TTPC concentration, entanglement of the fibers resulted in the formation of a supramolecular hydrogel. Investigation of the lyotropic mesophases in the TTPC supramolecular hydrogel showed the presence of multiple phases including two liquid crystal phases (*i.e.*, nematic and lamellar), which have a certain degree of structural order and are promising templates for constructing functional biomaterials.

Introduction

A nucleolipid is an amphiphilic molecule containing both a lipid and a nucleobase. The lipid, a major structural component of cellular membranes, acts as a boundary for compartmentalization and as a signal transduction medium for the regulation of cellular functions, while the nucleobase plays important roles in the storage and propagation of genetic information.[1] Hybrid nucleolipids combining lipids and nucleic moieties therefore have unique functions in biological processes. For example, cytidine diphosphate diacylglycerol,[2] a key intermediate in the biosynthesis of glycolipids and lipoproteins, and other naturally occurring nucleolipids in bacteria (tunicamycins, liposidomycins and septacidin) exhibit biological functions such as antifungal, antiviral or anti-tumor activity.[3,4]

The unusual molecular structure of nucleolipids also leads to unique characteristics within self-assembled structures. While the lipid component provides a mechanism for aggregation, the attached nucleobase facilitates non-covalent interactions among molecules.[5] Thus, these amphiphilic molecules self-assemble in aqueous or organic solution. The unique aggregation properties of nucleolipids are very attractive for the design of supramolecular assemblies with novel properties and for various potential applications.[6] Of particular interest are supramolecular hydrogels using nucleolipids as low molecular weight hydro-gelators (LMWHs).[7,8] The biological importance and biocompatibility of lipid and nucleic moieties make nucleolipid-based supramolecular hydrogels a candidate for bio-materials and artificial bio-devices for any potential bio-application, such as drug and gene delivery vehicles,[9–12] tissue engineering,[13] bio-diagnostics[14,15] and bio-therapeutics.[16–18] In nucleolipid-based supramolecular hydrogels, the hierarchical structure of LMWH-based hydrogels has inspired significant research with unique foci,[19] including the exploration of new artificial nucleolipid-LMWHs,[20] study of assemblies and gelation processes[21–23] and the properties of hydrogels,[24,25] all of which are of great importance to the development and application of nucleolipid-based biomaterials.[26]

Typically, to form non-covalent networks in supramolecular gels, the assemblies which are composed of amphiphilic molecules usually have one dimensional topologies (*e.g.* rods, fibers, tubes, helices *etc.*),[27] and the properties of the gels are closely related to those of the gel-components, or the gelators. While most of the efforts have focused on the design of artificial nucleolipids to create assemblies with distinct morphologies, for nucleolipid-based supramolecular hydrogels the mesophases in the gel sample have not been explored in depth. In particular, during the formation of supramolecular hydrogels involving the alternation of gelator concentration, different

[a] *Department of Chemical and Biological Engineering, University of Colorado Boulder, UCB 596, Colorado 80309, USA. E-mail: christopher.bowman@colorado.edu*
[b] *Materials Science and Engineering Program, University of Colorado Boulder, Boulder, Colorado 80309, USA*
[c] *Department of Physics, University of Colorado Boulder, Colorado 80309-0390, USA*
† Electronic supplementary information (ESI) available. See DOI: 10.1039/c8sm01383g

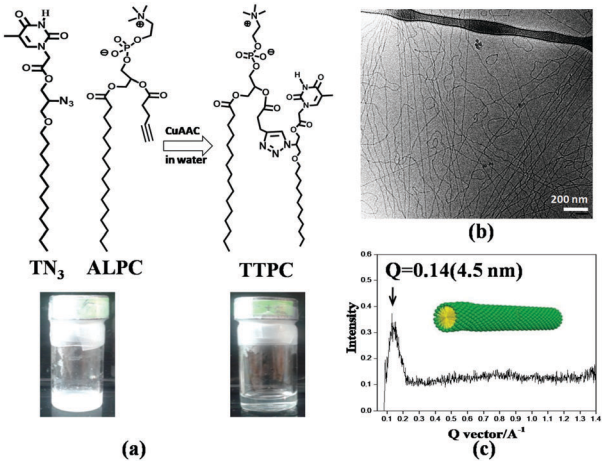

Fig. 1 (a) Conversion of alkyne lysolipid (AL) and thymine-containing azide (TN_3) precursors (0.5 mM) to thymine and triazole-phosphatidylcholine (TTPC) in the presence of sodium ascorbate and $CuSO_4$; the inset images show that the sample changes its appearance after CuAAC. (b) The cryo-TEM image of the TTPC-fibrous assembly in water. (c) 1-D SAXS curve of TTPC-fibers (5 mM TTPC in water) demonstrating that the fibers have a diameter of 4.5 nm. The inset is a cartoon illustration of the fibrous assembly.

lyotropic mesophases may be induced, and these mesophases are promising templates for functional constructs.

Here, a supramolecular hydrogel using an artificial nucleolipid containing a triazole ring, a thymine unit, and a phosphatidylcholine (TTPC) moiety was prepared. TTPCs were synthesized by coupling two precursors by a copper catalyzed azide alkyne cycloaddition (CuAAC) reaction in water (Fig. 1a), and the formed TTPC molecules self-assembled *in situ* into nanofibers. The morphology and driving forces of this fibrous assembly were investigated using a number of experimental methods, including cryo-transmission electron microscopy (cryo-TEM), nuclear magnetic resonance (NMR) spectroscopy, X-ray diffraction (XRD) and two-photon excitation fluorescence polarizing microscopy (2PEFPM). The supramolecular hydrogel was formed and different mesophases appeared when the concentration of TTPC was increased (Scheme 1). Meso-structured materials with different degrees of order have the potential for use as functional hydrogel materials.

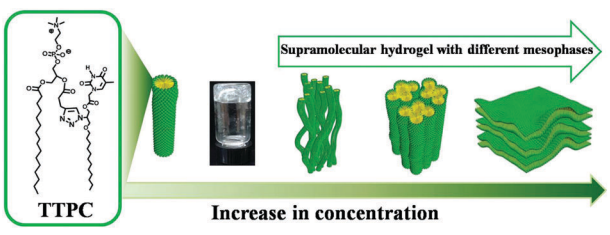

Scheme 1 Fibrous assembly formed by TTPC molecules in water. Increase in TTPC concentration resulted in a supramolecular hydrogel, and different lyotropic mesophases in the gel were induced by varying TTPC concentration.

Experimental

General procedure

Unless otherwise noted, all reactions were run under ambient conditions. All chemical reagents were obtained commercially and used without further purification. ^1H, ^{13}C NMR and 2-D hetero-nuclear single-quantum correlation (HSQC) NMR spectra were recorded on a Bruker Avance-III 400 spectrometer. Temperature-varied ^1H NMR data were recorded on a Varian Inova 400 spectrometer with an air-flow heating system. Fourier Transform Infrared (FTIR) spectra were recorded on a Nicolet 670 FT-IR spectrometer. Compound analysis and reaction monitoring were done using an analytical Agilent liquid chromatograph and mass spectrometer with a SedeX evaporative light scattering detector (LC-MS-ELSD), and an Agilent Zorbax Eclipse Plus C8 column was used for compound separation. Negative stain TEM imaging was carried out on a FEI Tecnai T12 Spirit, 120 kV LaB6 filament TEM. Cryo-TEM imaging was carried out on a FEI Tecnai F30, 300 kV FEG-TEM. Liquid crystal phases were examined using an Olympus polarized optical microscope (POM) equipped with a full wavelength retardation wave-plate and a hot stage. XRD tests were done using a diffractometer with a 30W XeocsGenix 3D X-ray source and a DectrisEiger R 1M detector.

Synthesis of a thymine-containing azide precursor

The synthesis of a thymine-containing azide precursor is described in the ESI,† Section 2.1 on the synthesis of a thymine-containing azide precursor.

Preparation of TTPC nanofiber assembly (*in situ* CuAAC) and supramolecular hydrogels

The alkyne lysolipid (AL, 1 eq.) and thymine-containing azide (TN_3, 1 eq.) were dispersed in water to obtain a 5 mM dispersion of precursors. Concentrated aqueous solutions of $CuSO_4$ (0.05 eq.) and sodium ascorbate (0.1 eq.) were added subsequently to catalyze the CuAAC reaction. The mixture was then incubated at room temperature for 12 hours. For gel preparation, to study the lyotropic mesophases, supramolecular hydrogels with different TTPC weight fractions were prepared. The TTPC fiber dispersion (5 mM, after CuAAC) was stirred and placed on a heating plate (40 °C) to evaporate water until different TTPC weight percentages were achieved. The gel samples were subsequently evaluated. Fluorescent dye ($DiOC_{18}$) was added to the precursor–dispersion to prepare fluorescent gel samples for 2PEFPM observation. For gel-samples containing GNRs, two precursors were distributed into GNR-containing aqueous dispersions. The CuAAC reaction was triggered and gel-preparation was performed as described.

Small angle X-ray scattering (SAXS)

SAXS experiments were conducted at room temperature. For gel samples, a flat sample holder was employed; for liquid samples, a capillary with 10 μm wall-thickness was used. A 30W Genix 3D X-ray generator (Cu anode, wavelength = 1.54 angstrom) was used and a beam of size 0.8 × 0.8 mm^2 was applied on all

samples ($\sim 4 \times 10^7$ photons per s flux was achieved in the beam). The DectrisEiger R 1M detector was used for data collection.

Two-photon excitation fluorescence polarizing microscopy (2PEFPM)

A gel sample with a fluorescent dye was placed on a glass slide and covered with a cover slip of 100 μm thickness. Imaging was performed by excitation with a 980 nm femto-second pulse from a tunable (680–1080 nm) Ti:sapphire oscillator (140 fs, 80 MHz, Chameleon Ultra-II, Coherent) and by detection with interference filters used to separate the fluorescent light from the excitation laser beam. A broad and half wave-plate (600–1200 nm) was used to change the polarization of the incident excitation laser beam.

Results and discussion

Design of precursors and CuAAC-mediated nanofiber formation

In addition to the ease of synthesis, the criterion for the design of a supramolecular gelator is the ability to disperse in an appropriate solvent (*i.e.*, one that facilitates self-assembly). Inspired by the work of Budin *et al.*,[28] in which they mimic cell membrane formation using a "click" chemical reaction, a thymine-containing azide precursor was designed and synthesized. The alkyne lysolipid was prepared with minor modifications to the previously reported procedure. The two precursors were coupled by a CuAAC reaction using a catalytic system of copper sulphate and sodium ascorbate. The coupled product, TTPC molecules, self-assembled into nanofibers almost immediately after formation. Pure TTPC molecules could not be well dispersed in the aqueous phase even at high temperature (80 °C).

The CuAAC-mediated self-assembly of nanofibers was confirmed by monitoring the CuAAC reaction using a liquid chromatograph equipped with a mass spectrometer and an evaporative light scattering detector (LC-MS-ELSD), while the fiber assembly was observed by cryo-TEM. LC-MS-ELSD traces revealed the consumption of the two precursors and accumulation of TTPC by the CuAAC reaction (Fig. S1, ESI†). The change in the appearance of the sample, from a turbid dispersion to a transparent viscous liquid, indicates the formation of distinct molecules and assemblies. Cryo-TEM images show that fibrous assemblies of diameter of ~4.5 nm formed *in situ* (Fig. 1b). Small-angle X-ray scattering (SAXS) data agree with the cryo-TEM image, with the strongest diffraction peak appearing at $Q = 0.14$ Å^{-1} (4.5 nm). Compared with previous research,[29] this measured diameter of 4.5 nm, which corresponds with other phospholipid assemblies of the bilayer structure, such as the DPPC bilayer in liposomes, indicates the end-to-end arrangement of the aliphatic chains of TTPCs in a fiber assembly.

Driving force in TTPC-nanofiber formation

The supramolecular assembly is formed through non-covalent interactions, such as van der Waals interactions, π–π stacking interactions, and hydrogen bonding. The TTPC molecules are amphiphilic, and contain a nucleobase and a triazole ring, all of which may be involved in the self-assembly process. To highlight their role in nanofiber assemblies, an NMR study was performed by adding varying amounts of water into a solution of TTPC in d_6-DMF (Fig. 2a). The addition of water leads to attenuation of the proton signals in a hydrophobic structure, such as the thymidine H-5′ proton and the triazole proton, indicating self-assembly of TTPCs;[13] moreover, the up-field shift of these two-proton signals verifies the contribution of both thymidine and triazole π–π stacking to the aggregation. With increased water fraction in the solution, the originally overlapping methine proton signals from the glycerol units gradually split (Fig. 2b), and the results from the 2-D HSQC NMR spectra confirm the up-field shifting signal belongs to the methine proton next to the triazole ring (Fig. S2, ESI†), which indicates the stacking of triazole rings in the TTPC nanofibers.[30] Thus, it may be concluded that a driving force for TTPC nanofiber assembly comes from a combination of hydrophobic/hydrophilic interactions, thymidine stacking and triazole ring stacking.

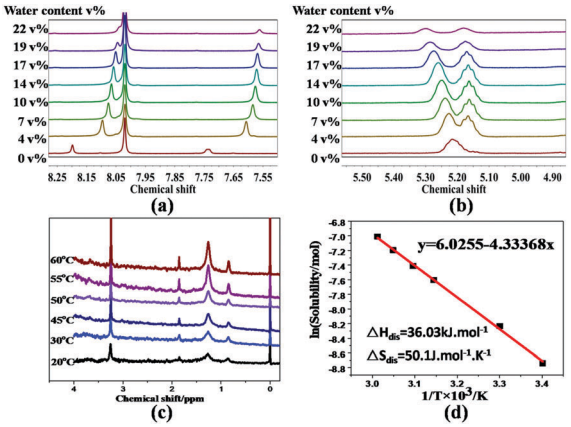

Fig. 2 Analysis of the driving forces for TTPC-fiber assembly, with the gradual addition of water into TTPC d_6-DMF solution. (a) Shift and attenuation of ^{1}H NMR signals (thymine H-5′ and triazole-H) verifying that stacking effects and hydrophobic forces facilitate TTPC assembly. (b) The splitting of the methane ^{1}H proton signals in the glycerol unit confirming triazole-ring stacking in the TTPC assembly. Thermodynamic analysis of the TTPC-nanofibrous assembly process, (c) traces of the temperature-varied ^{1}H NMR spectrum of TTPC in deuterium oxide showing that disassembly occurs when the temperature increases, during which more free TTPC molecules are soluble in D_2O and the signal intensity increases. (d) ΔH_{dis} and ΔS_{dis} calculated from the linear fit of ln(TTPC-solubility) *versus* inverse dissolution temperature.

Thermodynamic analysis of TTPC self-assembly

As documented in the literature, the self-assembly of amphiphilic molecules is governed by several contributing factors, including the molecular structure, solvent effects, concentration and temperature.[31,32] For a given solution of an amphiphilic compound in which a specific assembly exists, not all the amphiphilic molecules will be incorporated into the structured assemblies: some of the molecules will remain dissolved in the liquid-like solution phase. Different states of the amphiphilic molecules are monitored by NMR: proton signals of molecules

located in assemblies will be broadened and contribute minimally to the observed spectrum, whereas proton signals of the free molecules in solution will be detected and contribute most significantly to the integrated area and intensity of signals in the NMR spectrum. This simple NMR strategy was used to monitor the relative concentration of free-state molecules in the self-assembled TTPC-nanofibers. By varying the sample temperature, the change in NMR signal intensity was monitored, which corresponded to the concentration change of free TTPC molecules as a reflection of the self-assembly process. If we consider the disassembly process as analogous to the dissolution process, the solubility of TTPC can be expressed by the Van't Hoff equation,

$$\ln(\text{solubility}) = (-\Delta H_{dis}/RT_{eq}) + \Delta S_{dis}/R$$

in which ΔH_{dis} and ΔS_{dis} denote the molar enthalpy and the molar entropy for the disassembly process (the interconversion between assembly and free molecules), T_{eq} is the equilibrium temperature, and R is the gas constant. The proton signal of the repeating methylene ($-CH_2-$) was selected to calculate the relative concentration of free TTPC molecules at different temperatures (Fig. 2c), and a typical Van't Hoff plot is shown in Fig. 2d. ΔH_{dis} and ΔS_{dis} were calculated from the slope and intercept of the plot, and the opposite values of these two thermodynamic parameters reflect the change in enthalpy and entropy in the self-assembly process of TTPC molecules ($\Delta H_{as} = -\Delta H_{dis} = -36.03$ kJ mol^{-1} and $\Delta S_{as} = -\Delta S_{dis} = -50.1$ J mol^{-1} K^{-1}). Thus, the self-assembly of TTPC is an enthalpy-favored and entropy-disfavored process.

TTPC supramolecular hydrogel formation

The morphology of the TTPC assembly is fibrous and has the potential to form a gel by physical entanglement of the fibers. At room temperature (20 °C), the TTPC assembly dispersion forms a gel above a critical gel concentration (CGC) of 1.3 wt%. The gel exhibits typical rheological properties of a supramolecular gel, especially self-recovery, which is a common characteristic of supramolecular gels (Fig. S3 and S4, ESI†). To access the sol–gel transition temperature (T_{gel}) of the TTPC supramolecular hydrogel, we carried out a vial inversion experiment on gel samples with different TTPC concentrations. The T_{gel} value increases with higher TTPC concentration (from 1.3 wt% to 4 wt% TTPC), finally reaching a plateau ($T_{gel} \equiv 55$ °C when TTPC% >5 wt%) which denotes a concentration-independent T_{gel} (Fig. S5, ESI†).

Mesophases of TTPC supramolecular hydrogels

At room temperature a fibrous assembly forms at the critical aggregation concentration (CAC) of TTPC in water (0.00033 wt%, Fig. S6, ESI†), and this fibrous assembly morphology is maintained at all concentrations till gelation (CGC). An increase of the concentration of TTPC results in the appearance of birefringence which indicates the presence of liquid crystal (LC) ordering. At room temperature, POM images show that the LC phase appears at 5 wt% TTPC (Fig. 3a and b), and that gel samples with higher TTPC-fraction exhibit stronger birefringence. The birefringence

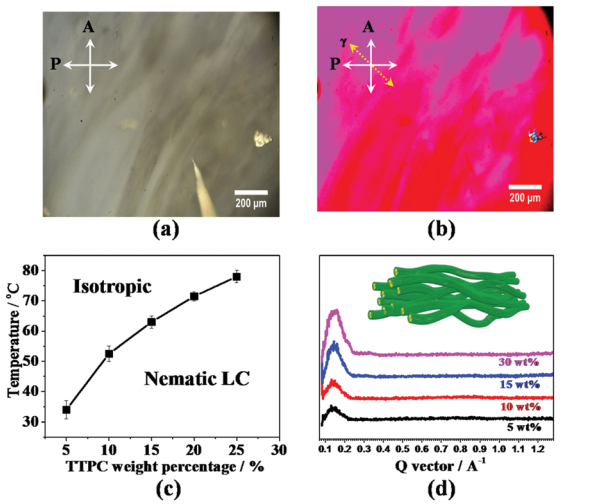

Fig. 3 POM images showing the formation of an LC phase in the 5 wt% TTPC sample, P: polarizer, A: analyzer. (a) Without and (b) with a full wavelength (530 nm) retardation wave-plate with slow axis (γ) marked with the yellow dash arrow. (c) The phase boundary of the TTPC gel sample (5–25 wt%). (d) 1-D SAX curves of TTPC gel samples illustrating that the lyotropic LC phase is composed of fiber bundles.

disappeared when the temperature increased (Fig. 3c), with a concentration-dependent LC-isotropic phase transition temperature, a characteristic of lyotropic LCs. To investigate the structure of this lyotropic LC, SAXS measurements were performed on gel samples with different TTPC-fractions ranging from 5 wt% to 30 wt%. The 1D SAXS spectrum shows only one diffraction peak, which has the same Q value as that corresponding to the diameter of the TTPC nanofiber (0.5 wt%) (Fig. 3d), indicating that the LC phase in gel-samples is likely composed of bundles of TTPC fibers (Fig. 3d).

For a detailed investigation of the LC phase, the sample was observed under 2PEFPM using a 25 wt% TTPC sample labelled with fluorescent dye $DiOC_{18}$ (Fig. 4a). The small diameter of the fibrous assembly induces high curvature at the transversal surface and leads to rotation–prohibition of the rigid oxacarbocyanine structure of $DiOC_{18}$ in the TTPC fiber,[33] resulting in the orientation of the oxacarbocyanine along the longitudinal axis of the nanofiber which is energetically favoured (Fig. 4b and c). The orientation of $DiOC_{18}$ reflects the alignment of the local director of the nematic fiber bundle $n(r)$. Due to the orientation of $DiOC_{18}$ molecules in the TTPC-fiber and the rotation–prohibition, the dye molecules show selective excitation and the fluorescence intensity exhibits a strong dependence on the polarization angle of the excitation light.[33] The influence of selective excitation lies in the intensity of fluorescence emission in 2PEFPM images. The intensity of the fluorescence signal in 2PEFPM imaging depends on the relative angular separation (θ) between the light polarization and the local director of the liquid crystal $n(r)$, scaling as $\sim\cos^4\theta$ for an unpolarized and as $\sim\cos^6\theta$ for a linearly polarized direction collinear with that of excitation light. The strong dependence on θ imparts a strong sensitivity of 2PEFPM to spatial variation in $n(r)$. Therefore, if the nematic fiber bundles exist, strongly polarization-dependent areas in the 2PEFPM images

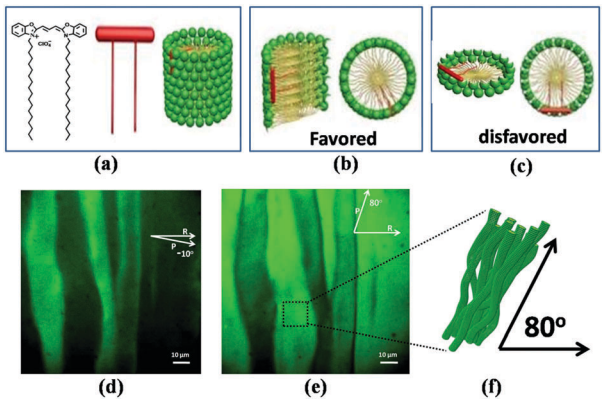

Fig. 4 (a) Illustrations of the chemical structure of $DiOC_{18}$ dye, and its location in a TTPC-nanofiber. The favoured (b) and disfavoured (c) alignment of the dipolar chromophore (oxacarbocyanine) of $DiOC_{18}$ in the TTPC-nanofiber. 2PEFPM images of TTPC gel samples (25 wt% TTPC, $DiOC_{18}$ as fluorescent dye) with linearly polarized excitation light at (d) −10 degrees and (e) 80 degrees to the reference angle (R = 0 degrees). (f) Orientation of the fiber-bundle parallel to the angle at which the strip has the strongest fluorescence intensity in the 2PEFPM image.

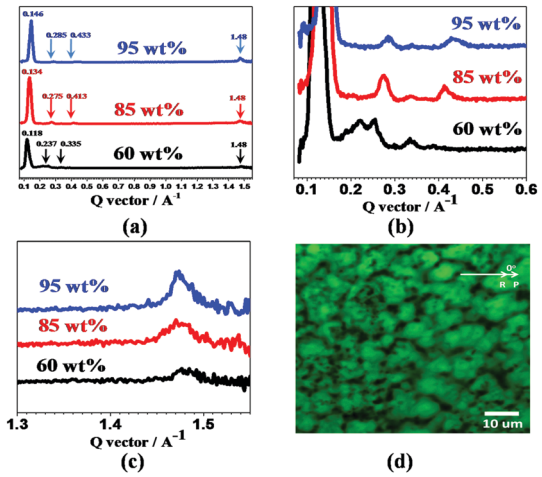

Fig. 5 (a and b) 1-D SAXS curves of high TTPC percentage gel samples (60 wt%, 85 wt%, 95 wt%). The main first order diffraction peak shows the period of the lamellar phase, and the second and third order harmonic diffraction peaks appear at higher Q values with minor intensity. (c) The wide-angle diffraction peak at 1.48 $Å^{-1}$ (0.425 nm) showing the alignment of the aliphatic chain of TTPC and the regular spacing between chains. (d) 2PEFPM image of the 85 wt% TTPC gel sample, which is not polarization dependent.

should be observed. As expected, in the 2PEFPM images, bright and dark strips were observed, and as we change the polarization angle of the excitation light, the fluorescence intensity of each strip changes (Fig. S7, ESI†). Specifically, a 90° change of the polarization angle gives an image in which the fluorescence intensity is complementary to the initial image (Fig. 4d and e). By measuring the fluorescence intensity as a function of polarization angle, information on the orientation direction of TTPC-fibers in a certain strip was obtained (Fig. 4f). The orientation of TTPC-fibers is parallel to the polarization direction at which the fluorescence intensity reaches its highest value. For TTPC gel samples with concentrations from the CAC to 35%, the TTPC assembly maintains the nanofiber morphology, and stacking of the TTPC-fibers results in a nematic LC phase and orientation of the fiber-bundles.

To investigate the changes in assembly and mesophases of the TTPC aqueous dispersion at higher concentration, gel samples with 60 wt%, 85 wt% and 95 wt% TTPC were analyzed by SAXS and 2PEFPM. In the high concentration samples of TTPC, the formation of lamellar phases was confirmed, and the lamellar period (first order diffraction) was indicated by the sharp fundamental diffraction peak in the range of 0.12–0.14 $Å^{-1}$. There are second and third harmonics between 0.2 and 0.5 $Å^{-1}$ (Fig. 5a and b), which indicate well-defined order in the samples (Table 1).

Decreasing the water content results in the shrinkage of the lamellar spacing, thus all the three diffraction peaks shift to higher Q values. Moreover, at the wide-angle diffraction area, a new diffraction peak emerges at 1.48 $Å^{-1}$ (0.425 nm) which corresponds with the spacing of aligned free fatty acid chains (Fig. 5c).[34]

To reveal the phase transition between the nematic LC phase (5–30 wt% TTPC) and the lamellar phase (60–95 wt% TTPC), two samples with TTPC concentrations of 40 wt% and 50 wt% were examined using XRD and 2PEFPM. SAXS results verify the presence of multiple phases. In the 1-D SAXS curve of

Table 1 X-ray diffraction data of high TTPC% gel samples

TTPC (wt%)	Small-angle diffraction peak (nm)			Wide-angle diffraction (nm)
	1st order	2nd order	3rd order	
60	5.32	2.65	1.87	0.425
85	4.68	2.28	1.52	0.425
95	4.30	2.20	1.45	0.425

the 50 wt% TTPC sample (Fig. 6a), three diffraction peaks appear in a small angle area: one at Q = 0.19 $Å^{-1}$ (3.3 nm); one at Q = 0.089 $Å^{-1}$ (7.05 nm); and one at Q = 0.114 $Å^{-1}$ (5.5 nm). The major diffraction peak (Q = 0.114 $Å^{-1}$, 5.5 nm) is almost the same as that of the lamellar phase from the 60 wt% TTPC sample (Q = 0.118 $Å^{-1}$, 5.32 nm), indicating formation of lamellar structures. In the 2PEFPM image of a 50 wt% TTPC sample, the fluorescence intensity detected from some areas is only weakly dependent on the polarization-angle of the laser excitation light (Fig. 6c and d, circled). These areas may be dominated by the lamellar phase in which the chromophore of the dye molecules is randomly distributed perpendicular to the lamellar plane (Fig. 6d, lamellar phase). Moreover, some of the stripe-shaped areas in 2PEFPM exhibit dependence on the linear polarization orientation-angle of the excitation light, which is consistent with the presence of fiber bundles, but no obvious diffraction peak was found at Q = 0.14 $Å^{-1}$ (4.5 nm) to represent TTPC fibrous assemblies (5–30 wt% TTPC). This outcome is likely associated with the dominance of the lamellar phase (Q = 0.118 $Å^{-1}$, 5.32 nm), and the diffraction peak of the fibers is easily overlapped by that of the lamellar phase due to small differences in the Q value. In the 1-D SAXS curve, another two diffraction peaks (Q = 0.089 $Å^{-1}$ and Q = 0.19 $Å^{-1}$) could not be attributed to any exact phases, but considering the assembly

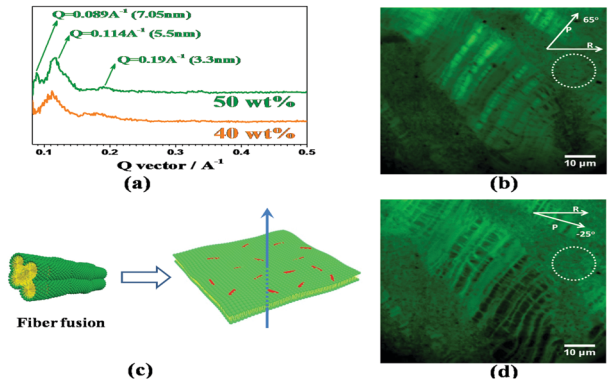

Fig. 6 (a) 1-D SAXS curves of gel samples of 40 wt% TTPC and 50 wt% TTPC, and appearance of new diffraction peaks indicating the coexistence of multiple phases. (b and d) 2PEFPM images of the 50 wt% TTPC gel samples confirming the coexistence of phases. Typical area in the white circle shows the lamellar phase which is less polarization-dependent. (c) Fiber fusion to form the lamellar phase, and random distribution of the chromophore of $DiOC_{18}$ in the lamellar plane: no orientation in the lamellar plane but perpendicular to the normal of the plane, resulting in reduced polarization dependence of the fluorescence intensity.

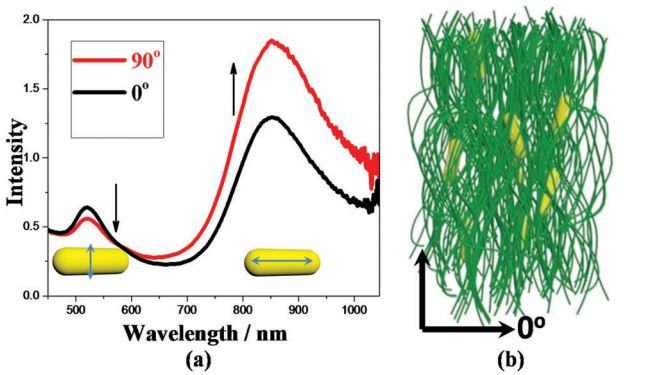

Fig. 7 (a) SPR spectrum change of GNRs in a TTPC supramolecular hydrogel, with polarized incident light at 0° and 90°, indicating that the GNRs are orientated in the gel sample. (b) Illustrative image of oriented GNRs in the TTPC gel sample.

structure of single TTPC fibers and the transition from fibrous bundles to the lamellar phase, it is hypothesized that the transition may involve fusion of fibers in a transversal direction (Fig. 6d), and the fusion induces phases with different periods, causing the two diffraction peaks. Although various defects appear across the fiber bundles, these defects are probably induced by fusion of fibers in the transition to the lamellar phase.

Investigation of the phase transition also reveals the lyotropic mesophase sequence in the TTPC supramolecular hydrogel. Upon increasing the TTPC concentration, the hydrogel exhibits a nematic LC phase formed by TTPC fiber bundles (5–30 wt% TTPC), a transitional phase (40–50 wt% TTPC), and a lamellar phase (60–95 wt% TTPC). All of these phases exhibit a certain degree of order at different scales, which enables them to be potential templates for constructing organic/inorganic composite materials.

Orientation of gold nanorods (GNRs) in a TTPC supramolecular hydrogel

To investigate the templating effect of the mesophase of the TTPC supramolecular hydrogel, a TTPC hydrogel (30 wt%) embedded with GNRs was prepared. The quaternary amine groups in the choline head of TTPC stabilizes GNRs in water, and due to the formation of the nematic LC phase and its orientation over micron-scale areas, GNRs were aligned along the director of the LC, resulting in a change in the surface plasmon resonance (SPR) spectrum (Fig. 7). The opposite behaviour of the transversal and longitudinal absorption peaks indicates the orientation of the GNRs by the nematic LC phase in the TTPC gel sample. The orientation of the nanofibers varies in different LC strips (Fig. 4e), thus, the SPR peak change shows the overall orientation effect of the LC phase on the GNRs, and in a single LC strip, the orientation of GNR is more pronounced. This result demonstrates that the alignment of GNRs in the TTPC gel is possible and relatively simple. These GNR-in-TTPC gel results show that the TTPC hydrogel mesophase is a promising template for the development of organic/inorganic functional biomaterial composites. In addition, the structural tenability of artificial nucleolipids enables a variety of self-assembled structures and may form new templating LC phases. Additional LC formation methods may provide tenability of LC phase formation, including approaches such as alignment-enhancement by applying electric or magnetic fields to control the orientation of the nematic phase, or a helical LC template produced by introducing chiral molecules into the gel-materials.

Conclusions

A new nucleolipid-based supramolecular hydrogel was prepared using triazole and thymine containing phosphatidylcholine molecules which self-assemble into nanofibers. At room temperature, the fibrous morphology of the TTPC assembly gels above 1.3 wt% TTPC and forms a nematic LC phase above 5 wt% TTPC. Increasing the TTPC concentration in the gel induces a phase transition which involves fusion of fibers, finally resulting in a lamellar phase. The gel sample in the nematic LC phase can induce the orientation of GNRs, providing a potential template for the construction of functional biomaterials.

Conflicts of interest

There are no conflicts to declare.

Acknowledgements

This work was supported by the U.S. Army Research Office (MURI program, Award W911NF-13-1-0383). The authors gratefully acknowledge the use of SAXS facilities and instrumentation supported by NSF MRSEC Grant DMR-1420736. Electron microscopy was performed at the University of Colorado,

Boulder EM Service Core Facility in the Dept. of MCDBiology, with the technical assistance of facility staff.

Notes and references

1 H. Rosemeyer, *Chem. Biodiversity*, 2005, **2**, 977–1063.
2 A. M. Heacock and B. W. Agranoff, *Biochim. Biophys. Acta*, 1997, **1348**, 166–172.
3 D. C. Hiss, G. A. Gabriels and P. I. Folb, *Cancer Cell Int.*, 2007, **7**, 5.
4 F. Van Tiel, W. Boere, T. Harmsen, C. Kraaijeveld and H. Snippe, *Antimicrob. Agents Chemother.*, 1985, **27**, 802–805.
5 S. Sivakova and S. J. Rowan, *Chem. Soc. Rev.*, 2005, **34**, 9–21.
6 V. Allain, C. Bourgaux and P. Couvreur, *Nucleic Acids Res.*, 2011, **40**, 1891–1903.
7 G. Godeau and P. Barthélémy, *Langmuir*, 2009, **25**, 8447–8450.
8 G. Godeau, J. Bernard, C. Staedel and P. Barthélémy, *Chem. Commun.*, 2009, 5127–5129.
9 P. Chabaud, M. Camplo, D. Payet, G. Serin, L. Moreau, P. Barthélémy and M. W. Grinstaff, *Bioconjugate Chem.*, 2006, **17**, 466–472.
10 S. Khiati, D. Luvino, K. Oumzil, B. Chauffert, M. Camplo and P. Barthélémy, *ACS Nano*, 2011, **5**, 8649–8655.
11 A. G. Kohli, P. H. Kierstead, V. J. Venditto, C. L. Walsh and F. C. Szoka, *J. Controlled Release*, 2014, **190**, 274–287.
12 L. Moreau, P. Barthélémy, Y. Li, D. Luo, C. A. Prata and M. W. Grinstaff, *Mol. BioSyst.*, 2005, **1**, 260–264.
13 L. Latxague, M. A. Ramin, A. Appavoo, P. Berto, M. Maisani, C. Ehret, O. Chassande and P. Barthélémy, *Angew. Chem., Int. Ed.*, 2015, **54**, 4517–4521.
14 E. Busseron, Y. Ruff, E. Moulin and N. Giuseppone, *Nanoscale*, 2013, **5**, 7098–7140.
15 A. Guerrero-Martínez, B. Auguié, J. L. Alonso-Gómez, Z. Džolić, S. Gómez-Graña, M. Žinić, M. M. Cid and L. M. Liz-Marzán, *Angew. Chem., Int. Ed.*, 2011, **50**, 5499–5503.
16 D. C. Drummond, O. Meyer, K. Hong, D. B. Kirpotin and D. Papahadjopoulos, *Pharmacol. Rev.*, 1999, **51**, 691–744.
17 R. Kanasty, J. R. Dorkin, A. Vegas and D. Anderson, *Nat. Mater.*, 2013, **12**, 967.
18 C. Wilson and A. D. Keefe, *Curr. Opin. Chem. Biol.*, 2006, **10**, 607–614.
19 J. Zhou, X. Du, Y. Gao, J. Shi and B. Xu, *J. Am. Chem. Soc.*, 2014, **136**, 2970–2973.
20 J. Huang, D. Ding, Z. Zhang, B. Shi and Y. Liang, *Synth. Commun.*, 1997, **27**, 681–690.
21 D. Berti, F. Baldelli Bombelli, M. Fortini and P. Baglioni, *J. Phys. Chem. B*, 2007, **111**, 11734–11744.
22 L. Moreau, P. Barthélémy, M. El Maataoui and M. W. Grinstaff, *J. Am. Chem. Soc.*, 2004, **126**, 7533–7539.
23 L. Moreau, M. Camplo, M. Wathier, N. Taib, M. Laguerre, I. Bestel, M. W. Grinstaff and P. Barthélémy, *J. Am. Chem. Soc.*, 2008, **130**, 14454–14455.
24 G. Godeau, C. Brun, H. Arnion, C. Staedel and P. Barthélémy, *Tetrahedron Lett.*, 2010, **51**, 1012–1015.
25 L. Latxague, M.-J. Dalila, A. Patwa, S. Ziane, O. Chassande, G. Godeau and P. Barthélémy, *C. R. Chim.*, 2012, **15**, 29–36.
26 X. Du, J. Zhou, J. Shi and B. Xu, *Chem. Rev.*, 2015, **115**, 13165–13307.
27 A. Gissot, M. Camplo, M. W. Grinstaff and P. Barthélémy, *Org. Biomol. Chem.*, 2008, **6**, 1324–1333.
28 I. Budin and N. K. Devaraj, *J. Am. Chem. Soc.*, 2012, **134**, 751–753.
29 L. J. Lis, M. McAlister, N. Fuller, R. P. Rand and V. A. Parsegian, *Biophys. J.*, 1982, **37**, 657–665.
30 M. J. Clemente, P. Romero, J. L. Serrano, J. Fitremann and L. Oriol, *Chem. Mater.*, 2012, **24**, 3847–3858.
31 X. Chi, A. J. Guerin, R. A. Haycock, C. A. Hunter and L. D. Sarson, *J. Chem. Soc., Chem. Commun.*, 1995, 2563–2565.
32 J. N. Israelachvili, D. J. Mitchell and B. W. Ninham, *Biochim. Biophys. Acta*, 1977, **470**, 185–201.
33 Q. Liu, C. Beier, J. Evans, T. Lee, S. He and I. I. Smalyukh, *Langmuir*, 2011, **27**, 7446–7452.
34 T. J. McIntosh, M. E. Stewart and D. T. Downing, *Biochemistry*, 1996, **35**, 3649–3653.